Supporting Information for:

Nanorod Position and Orientation in Vertical Cylinder Block Copolymer Films

Boris Rasin,[†] *Benjamin J. Lindsay,*[‡] *Xingchen Ye,*[§] *Jeffrey S. Meth,*[|] *Christopher B. Murray,* [†, §] *Robert A. Riggleman,*[‡] *and Russell J. Composto**[†]

[†]Department of Materials Science and Engineering, University of Pennsylvania, Philadelphia, Pennsylvania 19104, United States

[‡]Department of Chemical and Biomolecular Engineering, University of Pennsylvania, Philadelphia, Pennsylvania 19104, United States

[§]Department of Chemistry, University of Pennsylvania, Philadelphia, Pennsylvania 19104, United States

[|]DuPont Co., Wilmington, Delaware 19803, United States

Corresponding Author
*E-mail: composto@seas.upenn.edu.

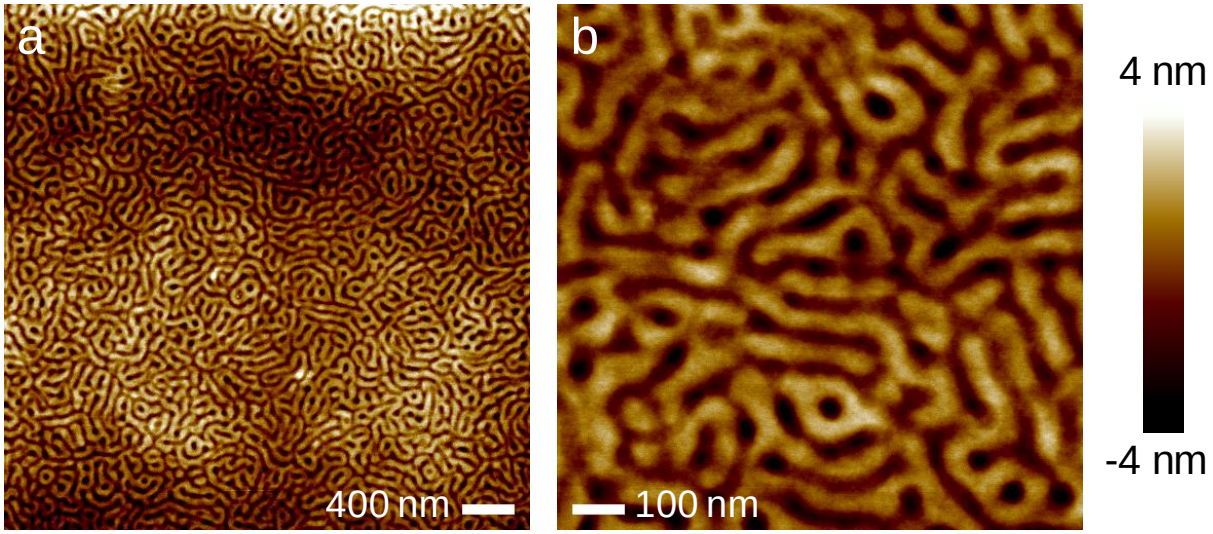

Figure S1. AFM topography images of neat as-spin-coated PS-*b*-P2VP films. (a) shows a 4 µm by 4 µm AFM topography image and (b) shows a 1 µm by 1 µm AFM topography image.

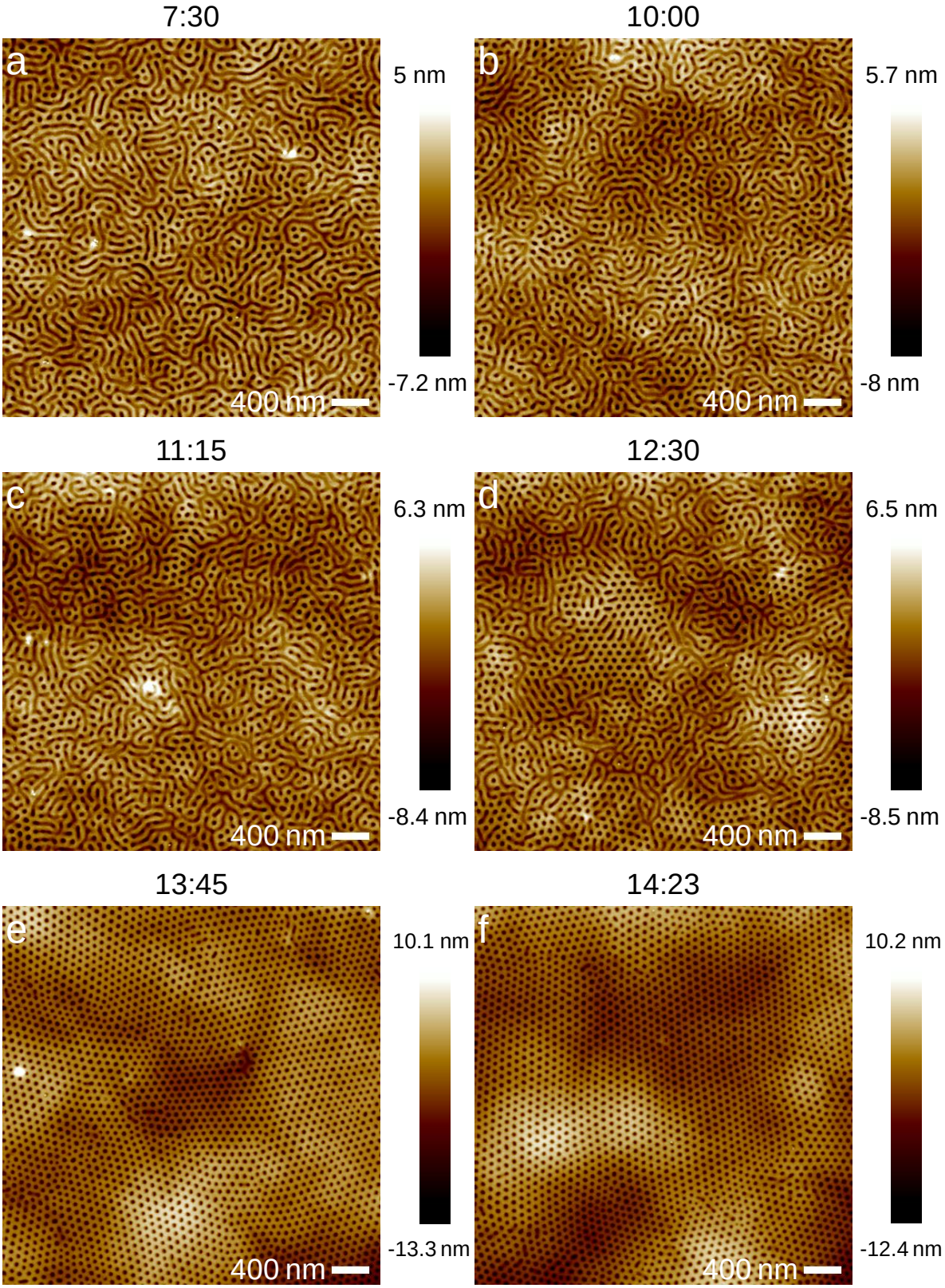
7:30
a
5 nm
-7.2 nm
400 nm
10:00
b
5.7 nm
-8 nm
400 nm
11:15
c
6.3 nm
-8.4 nm
400 nm
12:30
d
6.5 nm
-8.5 nm
400 nm
13:45
e
10.1 nm
-13.3 nm
400 nm
14:23
f
10.2 nm
-12.4 nm
400 nm

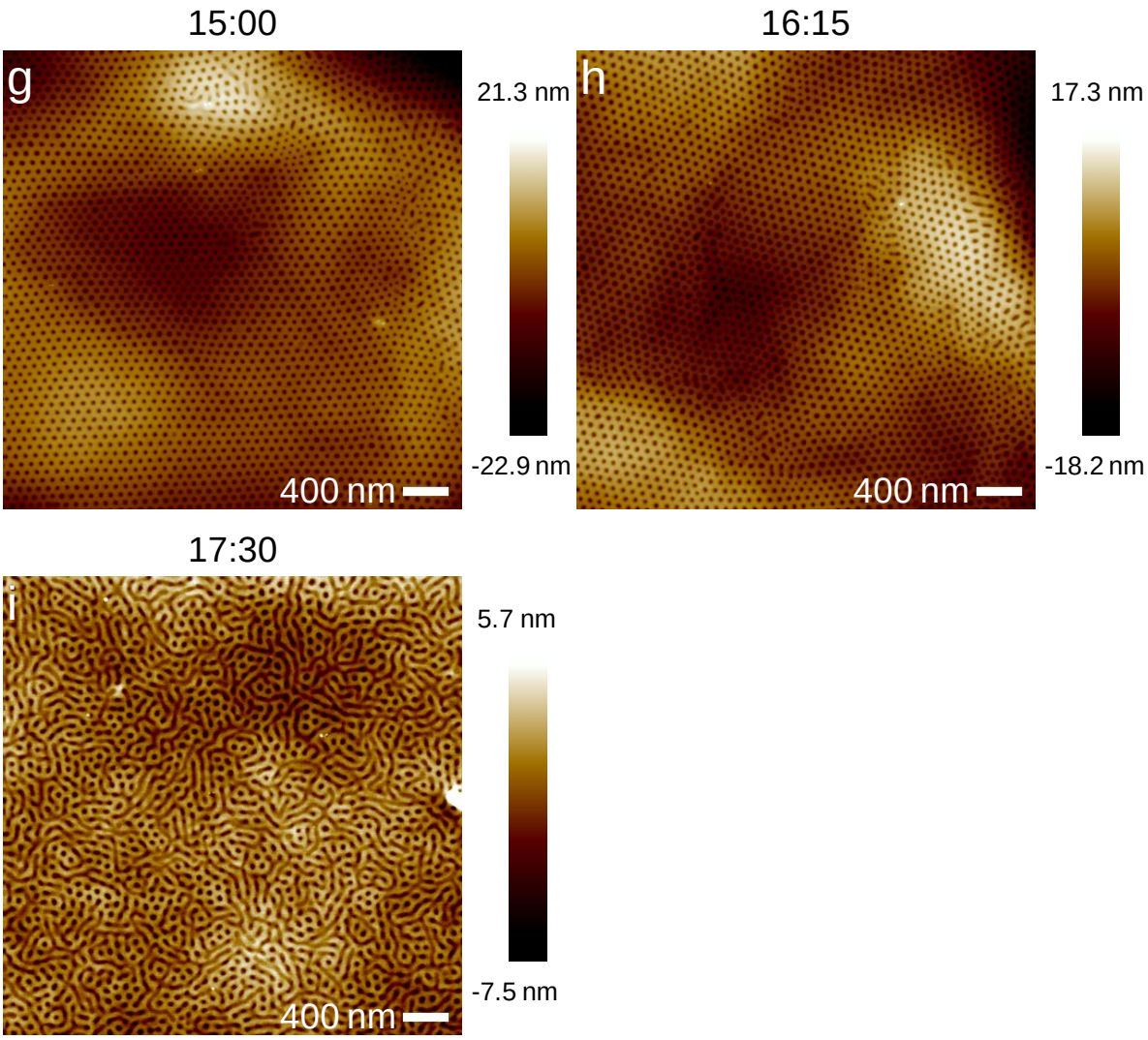

Figure S2. AFM topography images of neat PS-*b*-P2VP films solvent annealed in chloroform for various lengths of time. Above each AFM image the length of time the film in the image was solvent annealed is indicated in the format minutes:seconds.

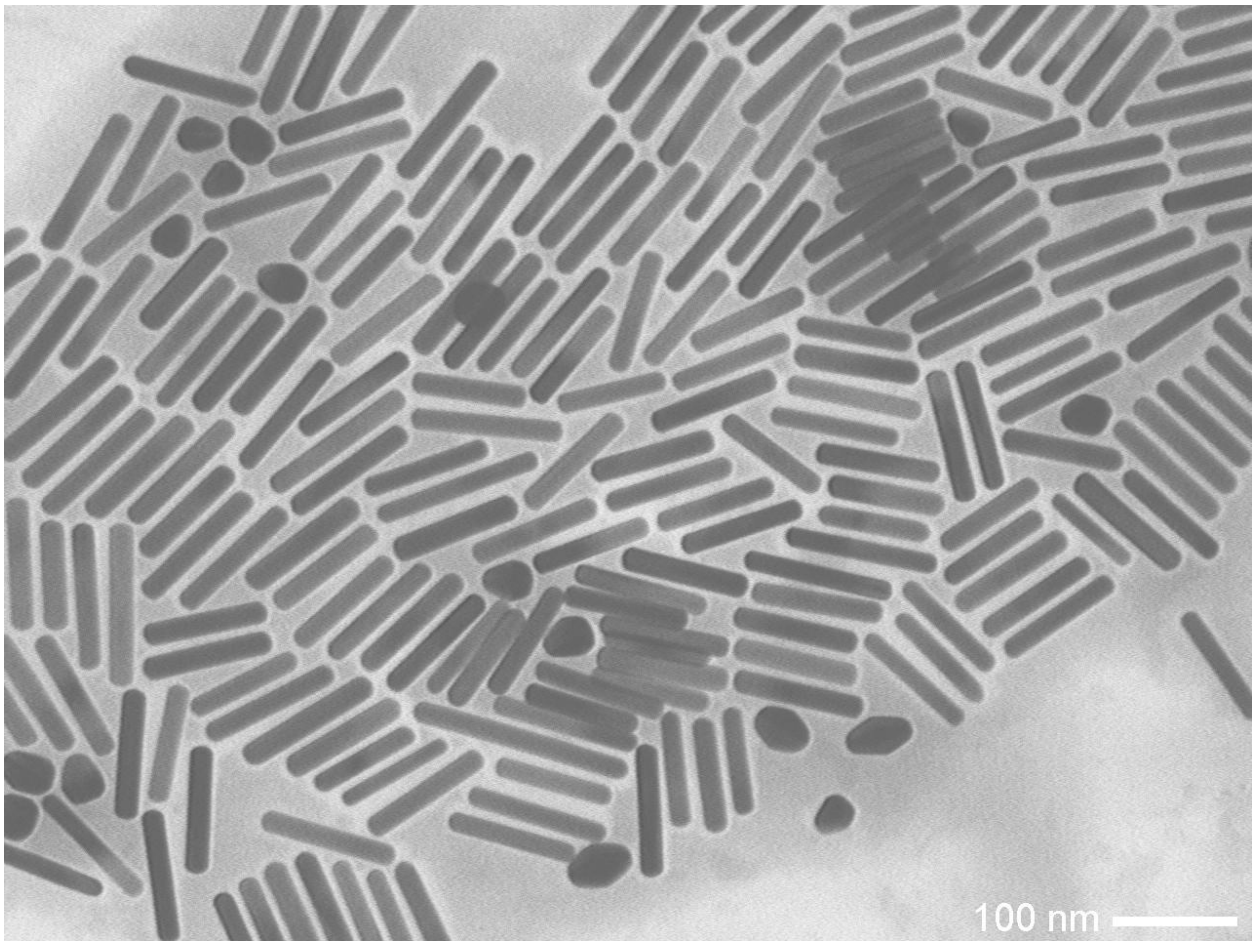

Figure S3. TEM image of the 101 nm length by 16 nm diameter gold nanorods.

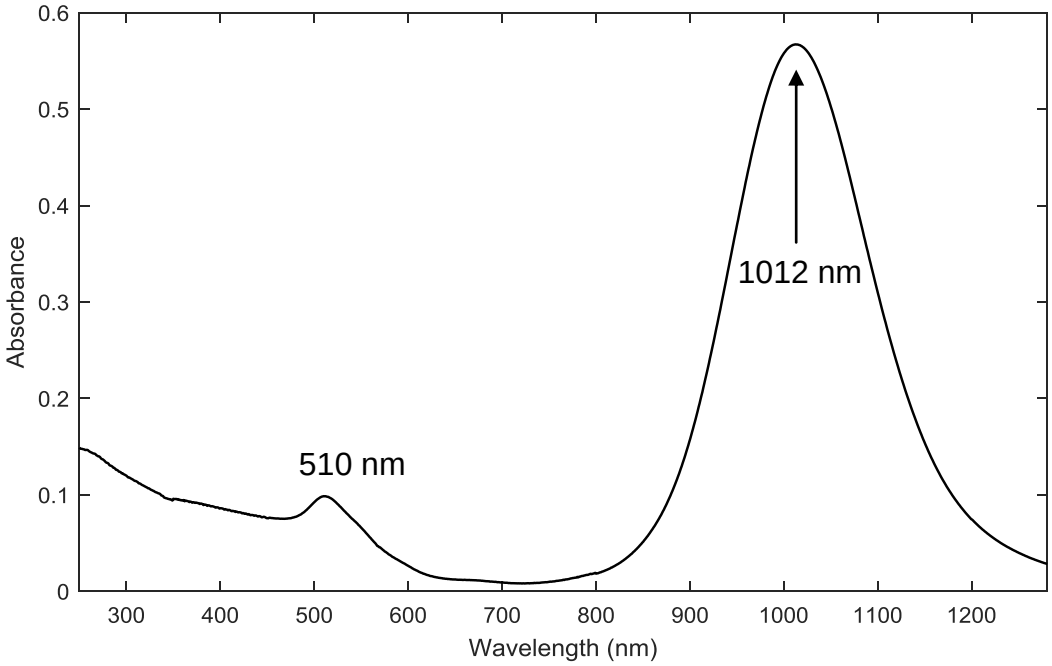

Figure S4. UV-vis-NIR spectrum of the 101 nm length by 16 nm diameter gold nanorods in water.

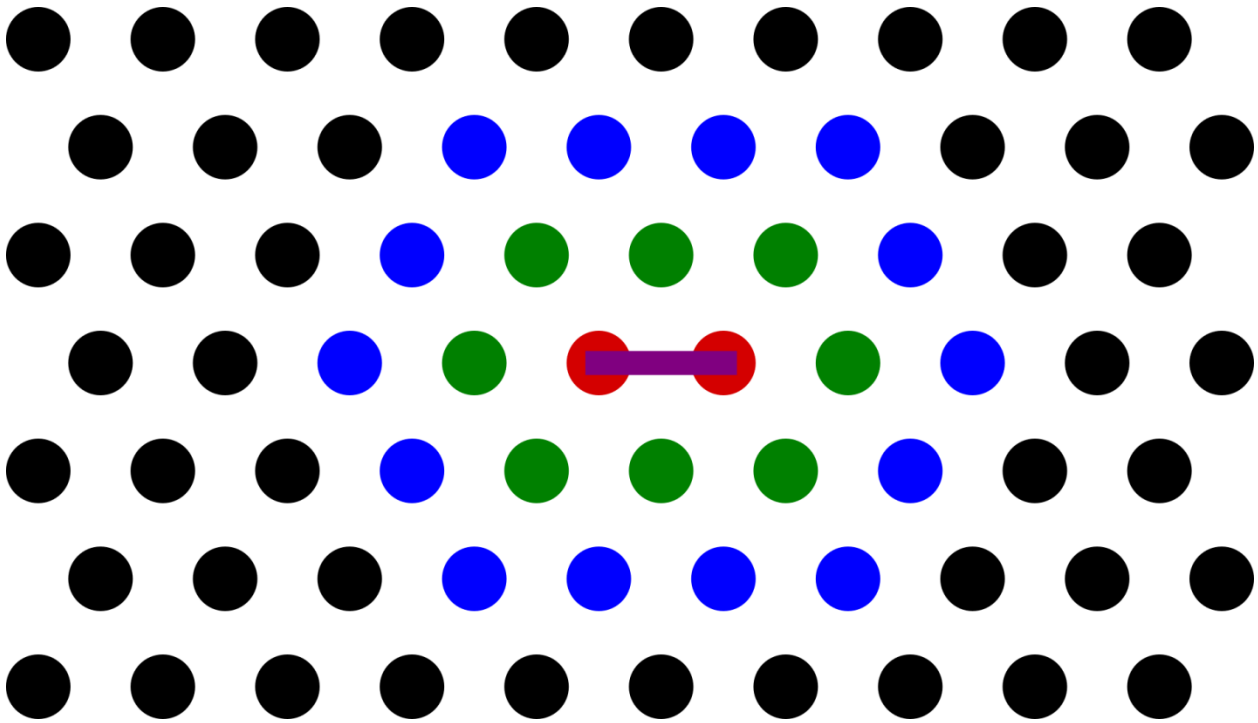

Figure S5. Diagram for identifying whether a gold nanorod in the bridging state is at a defect in the hexagonal lattice or is not at a defect in the hexagonal lattice.

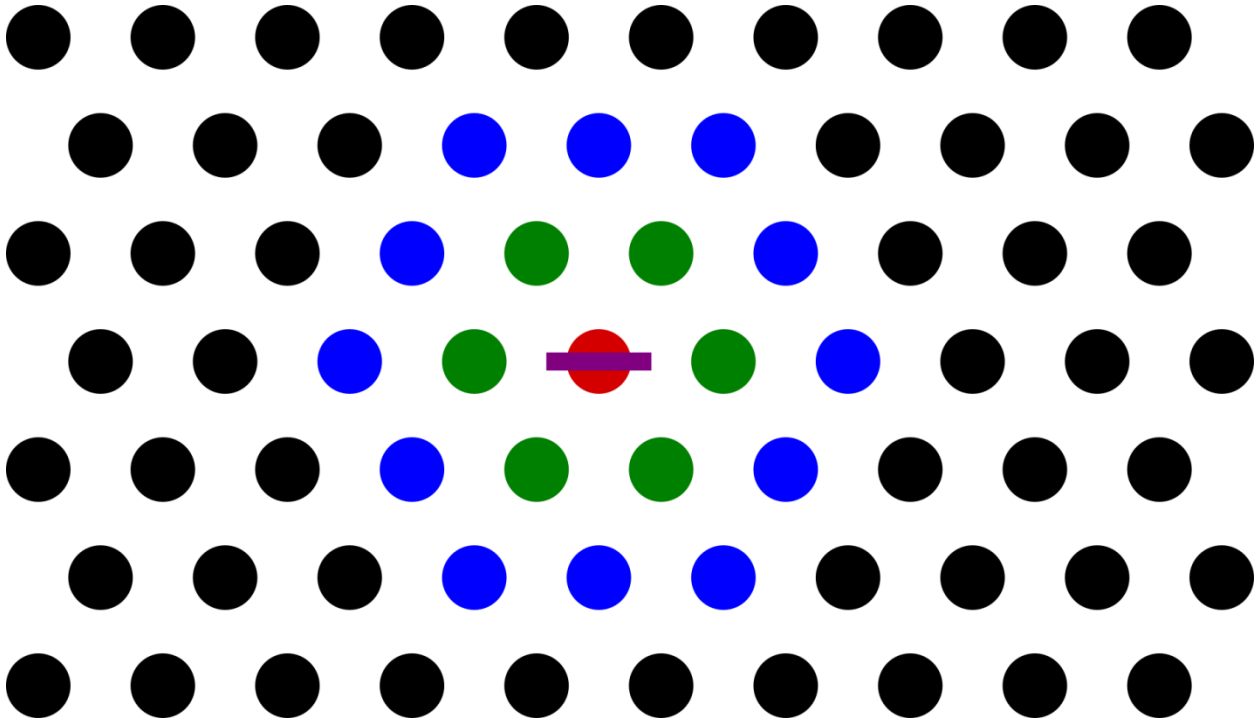

Figure S6. Diagram for identifying whether a gold nanorod in the centered state is at a defect in the hexagonal lattice or is not at a defect in the hexagonal lattice.

MODEL DETAILS

Thin cylindrical AB-diblock copolymer nanocomposite films were modeled with a modified version of the Hybrid Particle-Field Theory method developed by Sides and coworkers.[1] The primary modifications are that nanorods are modeled with an anisotropic function[2], surfaces are included as cavity functions to simulate the confinement seen in a thin film[3,4], and polymer segment mass is distributed by a Gaussian smearing function[2–4] with standard deviation of 0.2 R_g, where R_g is the ideal radius of gyration of the diblock copolymer. The diblock copolymer chains are represented as discrete Gaussian chains with $N = N_A + N_B$ segments, where the statistical segment sizes and monomer volumes of the two blocks are assumed to be identical.

The discrete Gaussian polymer chain connectivity is modeled using the harmonic bonding potential

$$\beta U_0 = \sum_i^{n_D} \sum_j^{N-1} \frac{3\left|\mathbf{r}_{i,j} - \mathbf{r}_{i,j+1}\right|^2}{2b^2} \tag{1}$$

where n_D is the number of diblock chains and b is the statistical size of a polymer segment. Density deviations away from the bulk density, ρ_0, are penalized using a Helfand compressibility potential, given by

$$\beta U_1 = \frac{\kappa}{2\rho_0} \int d\mathbf{r}\, [\hat{\rho}_+(\mathbf{r}) - \rho_0]^2 \tag{2}$$

where $\hat{\rho}_+ = \hat{\rho}_{DA} + \hat{\rho}_{DB} + \hat{\rho}_{NR} + \hat{\rho}_W$ is the spatially varying total density and κ controls the strength of the density fluctuations. In the limit $\kappa \to \infty$, the strictly incompressible model is recovered. $\hat{\rho}_{DA}$, $\hat{\rho}_{DB}$, $\hat{\rho}_{NR}$, and $\hat{\rho}_W$ are the microscopic densities of the A-block of the diblock chain, B-block of the diblock chain, nanorods, and confining surface, respectively. The nanorods are treated as having A-like chemistry and are described by the anisotropic function

$$\hat{\rho}_{NR}(\mathbf{r}) = \frac{\rho_0}{4} \mathrm{erfc}\left[\frac{|\mathbf{u}\cdot(\mathbf{r}-\mathbf{r}_c)| - L_{NR}/2}{\xi_{NR}}\right] \mathrm{erfc}\left[\frac{|\mathbf{u}\times(\mathbf{r}-\mathbf{r}_c)| - R_{NR}}{\xi_{NR}}\right] \tag{3}$$

where $\mathbf{u}$ is the unit vector pointing in the long direction of the nanorod, $\mathbf{r}_c$ is the position of the nanorod center, L_{NR} is the nanorod length, R_{NR} is the nanorod radius, and ξ_{NR} is the length scale defining the distance over which the nanorod density drops from ρ_0 to 0. The confining surface is a soft wall of thickness T_W on the bottom and top of the simulation box, and is neutral to both A and B chemistries. It is described by the function

$$\hat{\rho}_W(\mathbf{r}) = \frac{\rho_0}{2} \mathrm{erfc}\left[\frac{\min(r_z, L_z - r_z) - T_W}{\xi_W}\right] \tag{4}$$

where r_z is the z-component of $\mathbf{r}$, L_z is the box size in the z-dimension, and ξ_W is the length scale over which the surface drops from a density of ρ_0 to a density of 0. A and B components are assumed to interact through a purely repulsive, Flory-like contact potential given by

$$\beta U_2 = \frac{\chi}{\rho_0} \int d\mathbf{r} \left[\hat{\rho}_{DA}(\mathbf{r}) + \hat{\rho}_{NR}(\mathbf{r})\right] \hat{\rho}_{DB}(\mathbf{r}) \tag{5}$$

where the Flory parameter χ quantifies the magnitude of incompatibility between A and B components.

We assume that the mass of each polymer segment maintains a Gaussian distribution about its center, such that $\hat{\rho}_K(\mathbf{r})$, the microscopic density of polymer segment type K, is given by

$$\hat{\rho}_K(\mathbf{r}) = \int d\mathbf{r}' h(\mathbf{r}-\mathbf{r}') \hat{\rho}_{K,c}(\mathbf{r}') = (h * \hat{\rho}_{K,c})(\mathbf{r}) \tag{6}$$

where $\hat{\rho}_{K,c}(\mathbf{r})$ is the distribution of polymer segment centers given by

$$\hat{\rho}_{K,c}(\mathbf{r}) = \sum_i^{n_K} \sum_j^{N_K} \delta(\mathbf{r} - \mathbf{r}_{i,j}), \tag{7}$$

$h(\mathbf{r})$ is the Gaussian smearing function given by

$$h(\mathbf{r}) = \left(\frac{1}{2\pi a^2}\right)^{3/2} e^{-|\mathbf{r}|^2/2a^2} \tag{8}$$

where a is the smearing length scale (0.2 R_g in this work), and the last expression in Equation 6 introduces our shorthand notation for a convolution integral.

By employing a standard Hubbard-Stratonovich particle-to-field transformation, we arrive at a partition function

$$\mathscr{Z} = z_1 \int \mathscr{D}\{w\} e^{\mathscr{H}[\{w\}]} \tag{9}$$

where z_1 is a numerical prefactor containing the thermal de Broglie wavelengths and normalization constants from the Gaussian functional integrals used to decouple the particle interactions, and $\mathscr{H}$ is the effective Hamiltonian given by

$$\begin{aligned} \mathscr{H}[\{w\}] = \frac{\rho_0}{2\kappa} \int d\mathbf{r}\, w_+(\mathbf{r})^2 - i\rho_0 \int d\mathbf{r} w_+(\mathbf{r}) - \int d\mathbf{r} w_A(\mathbf{r}) \hat{\rho}_{NR} \\ + \frac{\rho_0}{\chi} \int d\mathbf{r} \left[w_{AB}^{(+)}(\mathbf{r})^2 + w_{AB}^{(-)}(\mathbf{r})^2 \right] - n_D \ln Q_D \left[\mu_A, \mu_B\right] \end{aligned} \tag{10}$$

Here, $\{w\}$ represents the set of chemical potential fields $w_{AB}^{(+)}(\mathbf{r})$, $w_{AB}^{(-)}(\mathbf{r})$, and $w_+(\mathbf{r})$; μ_A and μ_B are defined by $\mu_K = (h * w_K)(\mathbf{r})$ where

$$w_A = i\left(w_+ + w_{AB}^{(+)}\right) - w_{AB}^{(-)}, \tag{11}$$

$$w_B = i\left(w_+ + w_{AB}^{(+)}\right) + w_{AB}^{(-)}, \tag{12}$$

Q_D is the partition functions for a single diblock chain. Q_D is calculated iteratively from the chain propagator $q(j,\mathbf{r})$,

$$Q_D[\mu_A,\mu_B] = \frac{1}{V}\int d\mathbf{r}\; q(P,\mathbf{r}) \tag{13}$$

with the chain propagator constructed using a Chapman-Kolmogorov equation

$$q(j+1,\mathbf{r}) = e^{-\mu_K(\mathbf{r})}\int d\mathbf{r}\;\Phi(\mathbf{r}-\mathbf{r}')q(j,\mathbf{r}) \tag{14}$$

where K is either A or B depending on the type of segment $j+1$ and $\Phi(\mathbf{r}-\mathbf{r}')$ is the normalized bond transition probability.

The set of mean-field equations describing this system can be written as

$$\frac{\partial\mathscr{H}}{\partial w_K} = 0 \tag{15}$$

where w_K represents any field w_+, $w_{AB}^{(+)}$, or $w_{AB}^{(-)}$. To compute mean-field solutions, we evolve the fields according to

$$\left(\frac{\partial w_K(\mathbf{r})}{\partial t}\right) = -\lambda_K\left(\frac{\partial\mathscr{H}}{\partial w_K(\mathbf{r})}\right) \tag{16}$$

where λ_K is the relaxation coefficient for field w_K and t is a fictitious time. We use a first-order semi-implicit scheme[5] to numerically evolve the fields. For each free energy calculation, the vertical distance between the nanorod and the surface played a significant role in the resulting free energy since the interfaces are "soft", in that the surfaces of each are essentially a smoothed step function. In order to prevent this effect from dominating the free energy, the vertical position of the rod relative to the surface was chosen to minimize the free energy using Brent's method in each simulation. Figure S7 shows the free energy calculations for all 3 nanorod sizes tested.

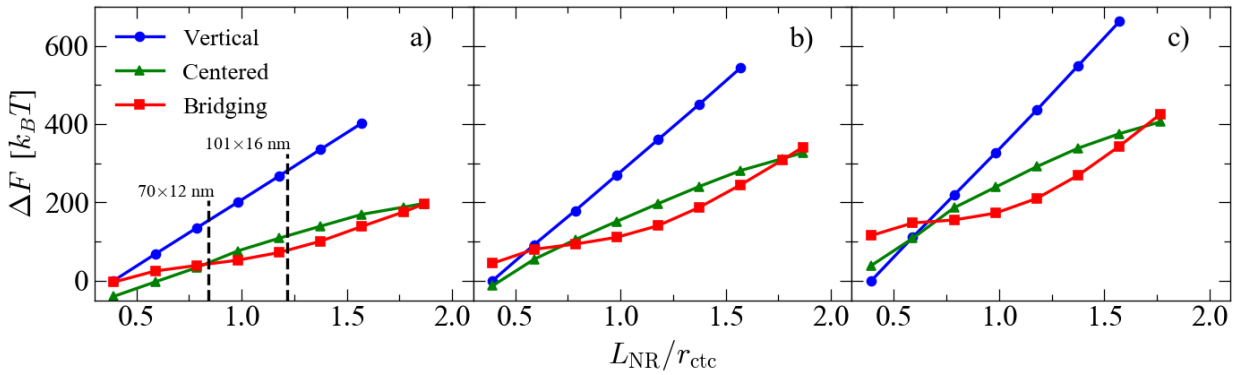

Figure S7. Mean-field free energy differences for nanorods in different configurations as a function of nanorod length for nanorods of diameter a) 1.0 R_g, b) 1.5 R_g, and c) 2.0 R_g. The nanorod length in the x-axis is normalized by the cylindrical domain nearest neighbor center-to-center distance, r_{ctc}. Free energy differences in each plot are calculated relative to the free energy of a rod of the same diameter in the vertical configuration with a length of 2 R_g, the shortest length in each case. The positions of the 101x16 nm and 70x12 nm rods used in experiments are marked in a) to show roughly where the experimental nanorod sizes fit into these calculations.

REFERENCES

[1]S. W. Sides, B. J. Kim, E. J. Kramer, and G. H. Fredrickson, Physical Review Letters **96**, 250601 (2006).

[2]J. Koski, H. Chao, and R. A. Riggleman, Journal of Chemical Physics **139**, 244911 (2013).

[3]H. Chao, B. A. Hagberg, and R. A. Riggleman, Soft Matter **10**, 8083 (2014).

[4]J. Koski, H. Chao, and R. A. Riggleman, Chem. Commun. **51**, 5440 (2015).

[5]E. M. Lennon, G. O. Mohler, H. D. Ceniceros, C. J. García-Cervera, and G. H. Fredrickson, Multiscale Modeling and Simulation **6**, 1347 (2008).